Effect of feedstock and plasma gun on the microstructure and bioactivity of plasma sprayed bioactive glass coatings

E. Cañas[1*], O. Rojas[2,3], M.J. Orts[1], H. Ageorges[2], E. Sánchez[1]

[1]Instituto de Tecnología Cerámica (ITC), Universitat Jaume I (UJI), Castellón, Spain

[2] Institut de Recherche sur les Céramiques (IRCER), Université de Limoges (UL), Limoges, France

[3]GIPIMME–GIMACYR, Universidad de Antioquía (UdeA), Medellín, Colombia

Eugeni Cañas Recacha Telephone number: (+34) 964342424

Email: eugeni.canas@itc.uji.es Fax number: (+34) 964342425

Óscar Iván Rojas Giraldo

Email: oscar.rojas@etu.unilim.fr

María José Orts Tarí

Email: mariajose.orts@itc.uji.es

Hélène Ageorges

Email: helene.ageorges@unilim.fr

Enrique Sánchez Vilches

Email: enrique.sanchez@itc.uji.es

Abstract

Plasma–sprayed 45S5 bioactive glass coatings were manufactured using two types of powder feedstocks (commercial and lab–made 45S5 glass) and two plasma torches (single and triple cathode) to analyse their influence on the microstructure and bioactivity of the coatings. Besides, the volatilisation of glass oxides such as Na_2O and P_2O_5 during the deposition was studied. All coatings were microstructurally characterised by scanning electron microscopy, X–ray diffraction and X–ray dispersive energy analysis. Moreover, the bioactivity of the sprayed coatings was studied by immersing the coatings in Simulated Body Fluid until 14 days.

The coatings obtained using the triple cathode torch showed similar thickness, less total porosity and greater microstructural homogeneity than the coating deposited with the single cathode torch. X–ray dispersive energy analysis revealed lower amounts of sodium and phosphorus at the surrounding of the lamellae, due to its volatilisation during the formation of the coatings. The volatilisation of these elements varied depending on the type of feedstock and plasma jet enthalpy. Concerning the bioactivity of the coatings, all of them have developed a hydroxycarbonate apatite layer on their surface.

Keywords: 45S5 bioactive glass; Powders; Bioactivity; Plasma spraying; Triple cathode torch

1. Introduction

Bioactive glasses have been widely studied as coatings onto metallic implants [1–4]. Atmospheric plasma spraying (APS), represents the most studied and used method for the deposition of this type of coatings [3,5–9]. This technique allows a perfect chemical and structural control of the resulting coating and hence control the properties of the coating only by tailoring the process parameters [2,5,10]. Moreover, this method enables the manufacture of coatings on a wide variety of implant's shapes, high deposition rates and high coating's thicknesses without thermally affecting the substrate [2,10].

During the last decades, the trend has been to obtain coatings with a finer microstructure by means of this technique, and therefore, improved properties [11]. One of the ways to achieve this type of microstructures is the utilisation of a multi–electrode plasma torch. The most used multi–electrode systems are two, one consisting of three different cathodes and a single anode, and the other one consisting of one cathode and three different anodes [12]. Basically, both multi–electrode systems give rise to a longer, more stable (with fewer fluctuations) and much more energetic plasma jet than that obtained with the conventional single–electrode system, even when monoatomic gases are used [11–17]. Therefore, the use of these multi–electrode systems leads to more molten particles with higher kinetic energy resulting in high deposition efficiency and improved coatings with denser microstructures compared to those deposited with a single–electrode torch [12].

Multi–electrode plasma torches have been used to deposit a wide variety of materials in different states (powders, suspensions and solutions) such as titania suspensions [18], yttria–stabilised zirconia suspensions [19,20], Fe–based powders [21,22], zirconyl nitrate solution [23] or alumina and titania + chromia powders [24]. Nevertheless, the deposition of bioactive glass coatings has been studied only with the conventional single–electrode plasma torch. To the best of our knowledge, there is no literature regarding the deposition of bioactive glasses by multi–electrode plasma torches.

In the present work, the influence of the different electrode systems on the microstructure and bioactivity coatings manufactured from bioactive glasses was studied. For that purpose, two bioactive glass powders (commercial and lab–made) with similar composition were deposited using both electrode systems, where the multi–electrode plasma torch employed is made up of three different cathodes and one anode. After coatings deposition, they were microstructurally characterised by field emission gun environmental scanning electron microscopy, X–ray diffraction and X–ray dispersive energy analysis to assess if an improvement in the resulting microstructure takes place without crystallisation and modification of the composition when changing from single–electrode to multi–electrode torch. Moreover, the same techniques were used with all coatings after being immersed in simulated body fluid for different times.

Understanding the influence of the multi–cathode system on the microstructural and biological characteristics of bioactive glass coatings will enable to establish the best conditions in the manufacture of these coatings for biomedical applications.

2. Experimental

2.1 Feedstocks

Two bioactive glass powders have been used as feedstocks for the manufacture of coatings by atmospheric plasma spraying (APS). The first one, with a composition close to 45S5, was synthesised in the laboratory by the melting and quenching method, which will be referred to as LBG (lab–made bioactive glass). The preparation details of this bioactive glass have been described elsewhere [25]. The second one was the commercial 45S5 bioactive glass (Schott Glass AG, Mainz, Germany) referred to as CBG (commercial bioactive glass) and described by Rojas et al. [6].

Table 1 shows the LBG and CBG chemical compositions. As observed, both compositions are very close. The LBG powder has a particle size under 63 μm [25], while the CBG has a particle

size under 40 μm [6]. Figure 1 displays the lab–made and commercial glass particles. Both feedstocks show the typical angular shape of melting–and–crushing glassy powders.

2.2 Coatings manufacture

Both powders were sprayed onto metallic substrates by APS. The substrates used were AISI type 304 stainless steel disks, as these are preliminary tests, with 25 mm of diameter. Previously to the deposition, the substrates were grit–blasted with corundum and cleaned in ethanol with ultra–sonic assistance. Then, to enhance the bioactive glass coatings' adhesion to the substrate [26], a TiO_2 bond coat was sprayed onto the metallic substrates using anatase (Metco 102, Oerlikon Metco, Switzerland) as feedstock with a particle size distribution from 10 to 55 μm. The bond coat deposition was made by atmospheric plasma spraying (APS) with a single cathode (SC) plasma torch (F4–MB, Oerlikon Metco, Switzerland) employing a powder flow rate of 45 g/min and a spraying distance of 120 mm, as suggested by the supplier. The rest of parameters used to deposit the bond coat, which were also given by the supplier, are showed in Table 2. Finally, the glass top coatings were manufactured using two different plasma torches, a single cathode plasma torch (F4–MB, Oerlikon Metco, Switzerland) and a triple cathode (TC) plasma torch (Triplex Pro–210, Oerlikon Metco, Switzerland) that broadens the operational range of the single cathode torch. The plasma–forming gas in the first torch (SC) was a mixture of argon as primary gas and hydrogen as secondary gas, while in the second torch (TC), argon was kept as primary gas, but helium was used as secondary gas. The parameters used to spray both glass powders are also given in Table 2. Regardless of the torch used, both glass powders were sprayed at the same spraying distance (100 mm), as well as were transported and fed into the plasma jet at the same flow rate (13 g/min) by pneumatic transport employing argon as the carrier gas.

With the SC torch, only one set of parameters was used, which has been chosen from previous studies. In this set, the proportion of hydrogen is relatively high to ensure a better melting of

the particles. Concerning the TC torch, two different sets of parameters were tried. On the first set (T1), a plasma jet with similar power to that obtained with the SC torch was accomplished by using argon and a small amount of helium (5 slpm of the 60 slpm of gases that form the plasma jet). The helium was added to increase the viscosity of the plasma jet and hence increase the residence time of the in–flight particles along the plasma jet. The second set of parameters (T2) resulted in a plasma jet with the same total flow rate of gases than that of the previous set but increasing the intensity of the electric arc resulting in a plasma jet with greater power.

2.3 Coatings characterization

The microstructure of the obtained coatings was observed in a field–emission gun environmental scanning electron microscope (FEG–ESEM) (QUANTA 200FEG, FEI Company, USA) with energy dispersive X–ray detector (EDX) (Genesis 7000 SUTW, EDAX, USA). The surface of the coatings and polished cross–sections were observed. Micrographs were taken at different magnifications using the backscattering signal detector under high vacuum conditions. Also, coatings thickness and porosity were estimated by image analysis (MicroImage) from FEG–ESEM cross–section micrographs at 2000x magnifications. 10 FEG–ESEM images were examined, and the findings averaged.

The amorphous/crystalline character of the coatings was determined by X–ray diffraction (XRD) (Advance diffractometer, Bruker Theta–theta, Germany). The XRD patterns were collected using Cu Kα radiation at a working power of 30 kV and 40 mA, a range of 2θ between 20º and 80º, a step size of 0.02º and a scanning speed of 0.5 s step^{-1}.

Finally, the surface roughness (3D roughness) of the coatings was evaluated with a confocal laser scanning microscopy (CLSM) (LEXT OLS5000, Olympus, Japan), using a stripped laser projection with a wavelength of 405 nm and a 10x magnification for data analysis recorder. The procedure followed to measure the roughness is described in a previous work [27].

2.4 SBF tests

In vitro test of the coatings was carried out following a standard protocol of immersing them in Simulated Body Fluid (SBF) [28].

SBF was prepared following the method of Professor Kokubo [29]. The coatings were immersed in SBF inside a plastic vessel that was maintained in a water bath at 36.5±0.5 ºC. Immersion times tested were 1, 7 and 14 days. After each time, the pH of the SBF was measured and the coated samples were removed from the vessel and gently washed with distilled water. Details of the experimental procedure have been written in a previous paper [30].

After that, the as–immersed coatings were dried, and to monitor compositional changes by EDX analysis when observing their surface morphology by FEG–ESEM. Besides, the formation of hydroxycarbonate apatite (HCA) was assessed by X–ray diffraction on the surface of the SBF tested coatings using the parameters set out in the previous section. FEG–ESEM observation was done using the secondary electron detector signal under high vacuum conditions at 2000x magnification.

3. Results and discussion

3.1. Microstructural characterization of the coatings

The average thickness and the total percentage of porosity of the manufactured coatings are presented in Table 3. The average thickness of all the coatings was the same, around 100 µm.

Regarding porosity, there were important differences in the total percentage of porosity of the coatings. The coating obtained with the single cathode torch (SC) displayed a total percentage of porosity double (27%) than that obtained in coatings manufactured with the triple cathode torch (TC) (11–12%), regardless of whether high (T2) or low power (T1) conditions have been used with the TC torch. When comparing the coatings obtained with the TC torch, no significant differences were found in any case regarding the total percentage of porosity. Therefore, the use of lab–made (LBG) or commercial (CBG) bioactive glass powders in high or low power

conditions does not seem to have a significant effect on the porosity rate. It should be pointed out that no other type of variables was tested, such as spraying distance or type of cooling of the substrate, which, according to the literature [6], also affect the porosity of the coatings.

Figure 2 shows the cross–section of the obtained bioactive glass coatings obtained with the single–cathode and tri–cathode plasma guns.

The coating prepared with the lab–made bioactive glass feedstock with the single–cathode torch (LBG–SC) (Figure 2a–b) shows an irregular surface, with valleys and sharp crests. In addition, the coating is composed of spherical pores, significant gaps between lamellae with irregular shape as well as dense areas of relatively wide extension. Those dense areas, with rounded boundaries, come from the larger LBG particles (see Figure 1a), which do not completely melt due to the short residence time of the in–flight particles within the hottest zone of the plasma jet as well as the low conductivity of the glass feedstock [31,32]. Consequently, the particle core remains unmelted and does not get flattened when it impacts the substrate. Concerning the spherical pores, this characteristic shape can be due to different factors. On the one hand, the high temperature of the plasma jet produces the volatilisation of the most volatile components, in this case, sodium and phosphorus, which implies a generation of gases that are released from the sample [6,33]. On the other hand, during the formation of the coating, the air could be trapped between the molten or semi–molten glass particles impacting on the substrate. The total occluded gases (air trapped + volatilised gas) could be removed if the viscosity of the melt was low enough to sinter by a viscous flow mechanism [34]. However, the fast cooling of the lamellae sharply increases the viscosity of the molten glass and prevents the removal of the air, leaving spherical pores in the coating.

Coatings of CBG manufactured with the SC torch are already published by *Rojas et al.* [6]. As it can be seen in this reference, lamellae are more flattened, stack better and no irregular gaps between lamellae can be found, only spherical pores. This is because of the lower particle size of this feedstock which causes a better melting of the particles. Besides, the thickness of the

coatings is lesser (around 60–70 µm) than that of the BG–SC coating. Nevertheless, despite the better stacking, volatilisation of sodium and phosphorus still occurs.

LBG coatings manufactured with the SC torch are thicker than those derived from the CBG powder, since particle size distribution is higher and hence particles don't get well flattened when they impact onto the substrate.

When the triple cathode torch (TC) is used to manufacture coatings with the LBG powder, even though the power of the plasma jet in T1 plasma conditions is the same as for those conditions of the SC torch, the kinetic energy transferred to the in–flight particles is higher due to an increase in argon flow rate. The effect of increasing the velocity of the particles on the microstructure is noticeable (Figure 2c–d). In these micrographs, the largest pores and the irregular gaps between lamellae are not observed, as was evident in those coatings deposited by SC, probably because the particles have experienced a higher plastic deformation due to their high velocity, retaining less volume of occluded gases. When the TC torch in high power conditions (T2 plasma conditions) is used both argon flow rate and plasma jet enthalpy increased, resulting in–flight particles with higher melting degree (lower viscosity of the molten particles) and higher velocity giving rise to pores with less size (Figure 2e–f). Regarding the dense areas with rounded boundaries, they are still present in coatings deposited from LBG feedstock with the TC torch, but to a lesser extent. These areas are still present in the TC coatings since they are the result of inadequate melting of larger glass particles because when spraying broader particle size distributions not all in–flight particles have the same thermo–kinetic treatment. Therefore, the raw material rather than the type of plasma gun used influences the correct stacking and homogeneity of the coatings.

When commercial bioactive glass powder (CBG) is used as a feedstock sprayed the TC gun (Figure 2g–h and 2i–j), the microstructure shows some changes concerning the LBG–T1 and LGB–T2 coatings. Firstly, the surface of the coating is more even, and the pores become a little smaller due to the finer glass particle size than the lab–made ones. Finer in–flight particles have

a higher thermokinetic treatment resulting in better stacking and outgassing due to the higher viscous flow. Likewise, other studies on ceramics [35–37] have shown that the smaller the initial particles, the more refined the structure of the material. Additionally, higher plasma power from TC torch leads to a better stacking and a homogeneous distribution of the pores (Figure 2i–j). It could be due to the fact that the CBG particles, melt even better (lower viscosity) in high power conditions. Consequently, in–flight glass particles release a more significant amount of occluded gases before impact and, when impacting on the substrate, they deform and adapt much better without occluding hardly any gas. On the other hand, part of the occluded gases may be removed by a viscous flow mechanism, as during the sintering of ceramic glazes [38].

At higher magnifications (Figure 2h and 2j), other details of the microstructure are revealed. The dense areas also appear in the coatings manufactured from the CBG feedstock. However, their boundaries become flattened instead of rounded and their size is significantly smaller than in the LBG coatings. Besides, as the TC torch provided more thermal and kinetic energy to in–flight glass particles than the SC torch, the CGB particles melt completely and retain their plastic character when hitting the substrate, giving rise to flat lamellae.

An effect of the plasma torch and the particle size distribution on the percentage and size pores was observed on the surface of coatings, as shown in Figure 3. This figure depicts the FEG–ESEM micrographs of the coating's surfaces, which are composed by lamellae of molten and semi–molten glass particles. The round pores present in the cross–section are also observed as well as longitudinal cracks due to the fast cooling and the thermal expansion mismatch between the glass and the substrate [6].

When comparing Figure 3a (LBG–SC) with Figures 3b (LBG–T1) and 3c (LBG–T2), LBG–T1 and LBG–T2 in addition to having less percentage of total porosity in the cross–section than LBG–SC, coatings manufactured by using the TC torch show a lower amount of big size pores and the appearance of very small pores on the surface. As mentioned above, probably this could

be due to the higher release of occluded gas because of the higher velocity of the glass particles when impacting the substrate. Regarding the coatings derived from the CBG feedstock, the pores are very small, and their percentage seems a bit higher than the three other coatings, probably not only due to the higher release of gases but also due to the smaller particle size.

The roughness (Sa) of the surface of the coatings was also measured. This parameter varied mainly as a function of the particle size distribution of the feedstock, while apparently, the type of plasma torch has no significant effect on this roughness parameter. The roughness of the coatings deposited with the LBG feedstock was 15.8 ± 0.8 µm. In comparison, the roughness of the coatings deposited with the CBG feedstock was 11.6 ± 0.6 µm, confirming that the coatings manufactured with the CBG feedstock are more even.

Moreover, performing a close examination of the micrographs taken with the backscattered detector, there is not a constant grey level in the microstructure of the coatings, suggesting differences in chemical composition inside them [6,39]. Thin, brighter, and flattened regions are seen surrounding darker regions in all the coatings. These regions can be easily observed in cross–section micrographs from Figure 2. Overall EDX analysis was also in coatings' cross–section by selecting low magnification areas that were representative of the microstructure and the results obtained are detailed in Table 4. The analysis shows depletion of sodium and phosphorus, volatilised during the flight of the glass particles in the plasma jet [6]. The differences in sodium and phosphorus are lower for the coating manufactured from the LBG using the SC torch than those for the coatings obtained with the same feedstock using the TC torch. The higher volatilisation of sodium and phosphorous with the TC torch is owing to the higher energy to which the glass particles are subjected. This is a consequence of the more excellent stability of the plasma jet of multi–cathode systems (TC torch), even when the plasma enthalpy is like that of monocathode systems (SC torch). It is also noted that in coatings sprayed by the TC gun under the same conditions but with different feedstock, the volatilisation increases when CBG is used. Indeed, the volatilisation takes place preferably at the surface of

the molten glass particles, but the volatilisation tends to be generated from the core of the glass particles as the size of the particles decreases, as in the case of the CBG particles. Consequently, coatings manufactured from smaller particles tend to have more significant changes in chemical composition.

From these results, it can be noticed that both the plasma torch and the particle size affect the volatilisation of sodium and phosphorus as described above. When coatings are sprayed with the TC torch, the plasma jet power affects the volatilisation of sodium and phosphorous, being higher in high power conditions. Regarding the particle size, although volatilisation occurs mainly on the surface and, to a lesser extent, from the particle core, this phenomenon depends on the energy per unit mass gained by in–flight particles, so the smaller the particle size, the greater the volatilisation. It is also evident that volatilisation is much higher in coatings deposited with the TC torch.

Finally, XRD spectra (see Figure 4) showed that all the obtained coatings displayed an amorphous character and no crystalline phases. The amorphous character remains since, although high temperatures are reached in the plasma plume to melt the glass particles, a fast cooling of the lamellae occurs when impacting on the substrate prevents the coating devitrification.

3.2. Bioactivity of the coatings: SBF tests

Figure 5 shows the surface of the coatings as–sprayed and after 1, 7 and 14 days of immersion in SBF. Changes in surface morphology of all coatings with immersing time evidence their interaction with SBF [8,30,40,41]. However, the rate and intensity of the reaction appear to be slightly different depending on the feedstock and the plasma torch. Initially, the glass surface leaches out the modifying ions (Na^+, Ca^{2+}) exchanging the alkali or alkali earth ions with protons of the liquid medium and a Si–rich layer is created [28]. Continuous leaching of ions from deeper and deeper areas and the dissolution of the glass in the liquid medium causes partial destruction of the glass network resulting in the development of numerous cracks on the coating

surface. The irregularities of this attacked glass surface act as nucleation sites where a layer rich in Ca and P is deposited from which hydroxycarbonate apatite (HCA) is formed. This HCA growth is observed by the development of spherical agglomerates, which increase in size and quantity with immersing time until they cover the entire surface and give the typical cauliflower–like appearance.

The micrographs in Figure 5 suggest that after one–day of immersing in SBF, regardless of the power condition applied, the coatings manufactured from the lab–made glass (LBG) with the TC torch are more reactive than the one sprayed by the SC torch, which seems to react at a lower rate. Thus, the coatings LBG–T1 and LBG–T2 show more surface cracks, which are indicative of increased ion exchange with the medium. This trend continues after 7 and 14 days of immersion. As far as the coatings obtained with the commercial bioactive glass powder (CBG) are concerned, they seem to react faster than the coatings obtained with the lab–made bioactive glass powder (LBG) as the newly formed HCA agglomerates are noticeable on the surface of the coating after a soaking time of 1 day. This trend continues until seven days, where the reaction seems to be completed since there are no significant differences in the amount and size of the HCA agglomerates formed between 7 and 14 days in both coatings (CBG–T1 and CBG–T2).

Generally, the bioactivity of a glass coating can be affected by many factors such as crystallinity, glass composition, roughness and specific surface area. On the one hand, in the present work all coatings have similar composition and are fully amorphous (see Figure 4), which cannot explain the differences. On the other hand, despite the fact that the coatings derived from the LBG powder are rougher than those derived from the CBG powder, the lamellae of the latter are smaller since the molten particles do not lose their identity when, after impact, they solidify on the substrate. In addition, as mentioned in section 3.1., it has been said that changing from the SC to the TC torch for the LBG feedstock, the surface of the coatings manufactured by the TC torch possessed a higher number of pores with small size than the

surface of the SC torch derived coating, resulting in coating surfaces with high specific surface area (both T1 and T2 plasma conditions). Concerning the CBG derived coatings, as said before, the surface of these coatings presented a higher percentage of pores which are even smaller in size than those of the LBG–TC coatings. Consequently, the specific surface area of the CBG–T1 and CBG–T2 coatings are the highest of the sprayed coatings.

Also, another factor that is probably affecting the bioactivity of the sprayed coatings to a lesser extent is the density of the coatings, that is, the amount of glass that exchanges ions. For a similar thickness (around 100 μm), the coatings sprayed by the TC torch have less percentage of total porosity. Therefore, these coatings have a higher amount of glass per unit of area, and hence they could be able to release a higher amount of ions.

The EDX spectra obtained when analysing the surface of as–sprayed coatings and after 1, 7, and 14 days of immersion in SBF show a gradual increase in the intensity of the Ca and P peaks and a decrease in that of the Na and Si peaks, either due to interaction with the medium, for Na, or to the growth of the HCA layer formed, for Si.

Figure 6 shows the EDX analysis spectra of the surface of the LBG–SC and LBG–T2 coatings as–sprayed and after an SBF soaking time of 14 days. When comparing these figures, the Si peak displays a much lower intensity in the coating obtained with the TC torch, which could be a signal that the thickness of the HCA layer formed is greater. These results confirm what was observed in Figure 5, that is, the LBG coatings sprayed by the TC torch are more reactive than that manufactured by the SC torch.

The diffraction patterns obtained for all coatings after 14 days of immersion in SBF reveals the peaks associated with the crystallisation of HCA (Figure 7 ~~8~~). All coatings display the same HCA peaks, even though the LBG–SC coating, as it is less reacted than the other coatings, displays less well–defined peaks (pattern from [42]).

Figure 8 shows the variation in the Ca and P content of the five coatings' surface, with the immersion time in SBF. These results have been obtained by analysing 0.134 mm^2 areas of the

surface of the coatings by EDX. As immersion time in SBF increases, the P content of the surface of the coatings also increases. This increase is very fast at the beginning and from 7 days becomes slow, being practically stabilised for 14 days of immersion. There is also a significant difference between the behaviour of the coatings sprayed by the SC and TC torches. In the coating manufactured by the SC torch, the increase in P content is lower, which corroborates its lower reactivity with SBF, probably because it is a less dense (high percentage of total porosity) coating with less specific surface area as mentioned above. In the other hand, there are no differences between the coatings obtained with the two power conditions of the TC torch. On comparing the curves corresponding to the coatings obtained from the two feedstocks with the triple cathode gun, the few differences observed in the structure of their surfaces are verified. Therefore, CBG coatings are generally more reactive than the LBG ones, which is probably due to the smaller pore size and surface roughness, hence higher specific surface area of the CBG derived coatings.

Concerning the variation of Ca with the immersion time in SBF, it is noticed that for the coating sprayed by the SC torch the curve is downwards, as it was with the P. Moreover, in this case, the concentration of Ca in the surface of the coating decreases initially for one day of immersion. This is due, as indicated in the literature [29,43], to the ion exchange with the medium, which is only noticeable before starting the HCA nucleation that increases the Ca concentration in the coatings' surface. In the coatings sprayed by the TC torch, the initial reduction of the calcium concentration is not appreciated, which could be since it can occur in less than one day since as mentioned above, these coatings are more reactive. Contrary to what happened for P, no significant differences in the calcium variation of the coatings obtained with the two feedstocks can be seen, which allows us to conclude that their reactivity is quite similar. More research is being carried out to determine the adherence of the coatings to the substrate and the growth rate and thickness of the HCA layer on the coating's surface. Besides, it is

necessary to optimise the spraying parameters to preserve as far as possible the obtained microstructures and reduce the volatilisation of sodium and phosphorus.

4. Conclusions

Two bioactive glass powders have been used, one lab–made (LBG) and the other commercial (CBG), to obtain coatings by APS using two plasma torches: single–cathode (SC) torch and triple–cathode (TC) torch. The starting glasses had different particle size distribution (LBG <63 μm and CBG <40 μm) so the effect of the feedstock particle size and the plasma gun power on the coating's microstructure have been studied.

Regardless of the torch or the glass powder employed, XRD spectra revealed that all coatings were amorphous. Coatings deposited with the TC torch, regardless of the power conditions used, have a more homogeneous and denser (less total percentage of porosity) microstructure than that prepared with the SC torch. It has been found that the percentage and size of the pores of the coatings depend on the particle size of the feedstock and on the plasma torch used since the higher thermal and kinetic energy supplied to the particles by the TC torch give rise to a better melting degree of the glass particles and a better stacking of the glass particles when they impact onto the substrate. However, the high temperature of the plasma torch causes volatilisation of sodium and phosphorus from the surface of the molten feedstock particles. This evolved gas results in an additional source of pores in the coating. It has been found that this volatilisation increases with the power of the plasma and by decreasing the size of the feedstock particles. That is, it is higher for coatings obtained with the TC torch from commercial bioactive glass, under high power conditions.

All coatings have reacted with SBF, although there are differences in the kinetics at which the HCA formation takes place, due to the differences in the specific surface area between the sprayed coatings. Using the same kind of feedstock, changing from the SC torch to the TC torch results in coating surface with higher specific surface area and a hence higher rate of reaction

with SBF. Moreover, the specific surface area of the coating's surface could be improved by reducing the particle size of the feedstocks, therefore enhancing the bioactivity of the coatings. For a 14–day SBF immersion period, however, all coatings had carbonated hydroxyapatite (HCA) layer, as verified on the surface by XRD analysis, regardless of the feedstock and the plasma torch used to manufacture them.

Based on the above, it can be concluded that the TC torch could be a suitable plasma torch to deposit bioactive glass coatings. The coatings sprayed by the TC torch preserved the amorphous character of the feedstocks and the resulting microstructures were enhanced regarding the one obtained with the SC torch. Additionally, the coatings sprayed by the TC torch showed higher bioactivity, identified with the HCA formation and the changes in the ionic composition of calcium and phosphorus, even up to 14 days of exposure to SBF.

Acknowledgements

The authors of the present work thank Universitat Jaume I of Castellón the support provided in funding action 2 (E–2018–20) and action 3.1. (PREDOC/2015/50) of the Research Promotion Plan, and the Administrative Department of Science, Technology and Innovation (COLCIENCIAS) of Colombia the support provided in funding Project 1115745–57862 and 727 doctoral scholarship.

References

[1] F. Baino, E. Verné, Glass–based coatings on biomedical implants: a state–of–the–art review, Biomed. Glasses 3 (2017) 1–17.

[2] J.R. Jones, A.G. Clare, Bio–glasses. An introduction, 1st ed., John Wiley & Sons, Great Britain, 2012.

[3] A. Sola, D. Bellucci, V. Cannillo, A. Cattini, Bioactive glass coatings: a review, Surf. Eng. 27 (2011) 560–572.

[4] M.H. Fathi, A. Doostmohammadi, Bioactive glass nanopowder and bioglass coating for biocompatibility improvement of metallic implant, J. Mater. Process. Technol. 209 (2009) 1385–1391.

[5] R. Sergi, D. Bellucci, V. Cannillo, A comprehensive review of bioactive glass coatings: State of the art, challenges and future perspectives, Coatings 10 (2020) 757.

[6] O. Rojas, M. Prudent, M.E. López, F. Vargas, H. Ageorges, Influence of atmospheric plasma spraying parameters on porosity formation in coatings manufactured from 45S5 Bioglass® powder, J. Therm. Spray Techol. 29 (2020) 185–198.

[7] G. Bolelli, D. Bellucci, V. Cannillo, R. Gadow, A. Killinger, L. Lusvarghi, P. Müller, A. Sola, Comparison between suspension plasma sprayed and high velocity suspension flame sprayed bioactive coatings, Surf. Coat. Technol. 280 (2015) 232–249.

[8] M. Monsalve, H. Ageorges, E. Lopez, F. Vargas, F. Bolivar, Bioactivity and mechanical properties of plasma–sprayed coatings of bioglass powders, Surf. Coat. Technol. 220 (2013) 60–66.

[9] V. Canillo, A. Sola, Different approaches to produce coatings with bioactive glasses: enamelling vs plasma spraying, J. Eur. Ceram. Soc. 30 (2010) 2031–2039.

[10] J. Henao, C. Poblano–Salas, M. Monsalve, J. Corona–Castuera, O. Barceinas–Sánchez, Bio–active glass coatings manufactured by thermal spray: a status reports, J. Mater. Res. Technol. 8 (2019) 4965–4984.

[11] A. Vardelle, C. Moreau, N.J. Themelis, C. Chazelas, A perspective on plasma spray technology, Plasma Chem. Plasma Process. 35 (2015) 491–509.

[12] J.L. Marqués, G. Forster, J. Schein, Multi–electrode plasma torches: Motivation for development and current state–of–the–art, The Open Plasma Phys. J. 2 (2009) 89–98.

[13] J. Schein, M. Richter, K.D. Landes, G. Forster, J. Zierhut, M. Dzulko, Tomographic investigation of plasma jets produced by multielectrode plasma torches, J. Therm. Spray Technol. 17 (2008) 338–343.

[14] K. Bobzin, N. Bagcivan, I. Petkovic, Numerical and experimental determination of plasma temperature during air plasma spraying with a multiple cathodes torch, J. Mater. Process. Technol. 211 (2011) 1620–1628.

[15] J. Schein, J. Zierhut, M. Dzulko, G. Forster, K.D. Landes, Improved plasma spray torch stability through multi–electrode design, Contribution Plasma Phys. 47 (2007) 498–504.

[16] J. Mostaghimi, M.I. Boulos, Thermal plasma sources: How well are they adopted to process needs?, Plasma Chem. Plasma Process. 35 (2015) 421–436.

[17] D. Zhang, L. Zheng, X. Hu, H. Zhang, Numerical studies of arc plasma generation in single cathode and three–cathode plasma torch and its impact on plasma spraying, Int. J. Heat Mass Transf. 98 (2016) 508–522.

[18] E. Bannier, G. Darut, E. Sánchez, A. Denoirjean, M.C. Bordes, M.D. Salvador, E. Rayón, H. Ageorges, Microstructure and photocatalytic activity of suspension plasma sprayed TiO_2 coatings on steel and glass substrates, Surf. Coat. Technol. 206 (2011) 378–386.

[19] P. Sokolowski, P. Nylen, R. Musalek, L. Latka, S. Kozerski, D. Dietrich, T. Lampke, L. Pawlowski, The microstructural studies of suspension plasma sprayed zirconia coatings with the use of high–energy plasma torches, Surf. Coat. Technol. 318 (2017) 250–261.

[20] D. Waldbillig, O. Kesler, The effect of solids and dispersant loadings on the suspension viscosities and deposition rates of suspension plasma sprayed YSZ coatings, Surf. Coat. Technol. 203 (2009) 2098–2101.

[21] X.Q. Liu, Y.G. Zheng, X.C. Chang, W.L. Hou, J.Q. Wang, Z. Tang, A. Burgess, Microstructure and properties of Fe–based amorphous metallic coating produced by high velocity axial plasma spraying, J. Alloy. Compd. 484 (2009) 300–307.

[22] K. Bobzin, N. Kopp, T. Warda, I. Petkovic, M. Schaefer, K.D. Landes, G. Forster, S. Zimmermann, J.L. Marqués, S. Kirner, M. Kauffeldt, J. Schein, Particle in–flight and coating properties of Fe–based feedstock materials sprayed with modern thermal spray systems, J. Therm. Spray Technol. 22 (2013) 363–370.

[23] D. Soysal, C. Christenn, A. Ansar, Process development for nanostructured functional layers by liquid injection plasma spraying for solid oxide fuel cells, ECS Transactions 25 (2009) 601–610.

[24] K. Bobzin, W. Wietheger, M.A. Knoch, A. Schacht, Heating behaviour of plasma sprayed TiO_x/Cr_2O_3 coatings for injection moulding, Surf. Coat. Technol. 399 (2020) 126199.

[25] E. Cañas, M. Vicent, E. Bannier, P. Carpio, M.J. Orts, E. Sánchez, Effect of particle size on processing of bioactive glass powder for atmospheric plasma spraying, J. Eur. Ceram. Soc. 36 (2016) 837–845.

[26] G. Goller, The effect of bond coat on mechanical properties of plasma sprayed bioglass–titanium coatings, Ceram. Int. 30 (2004) 351–355.

[27] V. Carnicer, M.J. Orts, R. Moreno, E. Sánchez, Engineering zirconia coating microstructures by using saccharides in aqueous suspension plasma spraying feedstocks, Ceram. Int. 46 (2020) 23749–23759.

[28] A.L.B. Maçon, T.B. Kim, E.M. Valliant, K. Goetschius, R.K. Brow, D.E. Day, A. Hoppe, A.R. Boccaccini, I.Y. Kim, C. Ohtsuki, T. Kokubo, A. Osaka, M. Vallet–Regi, D. Arcos, L. Fraile, A.J. Salinas, A.V. Teixeira, Y. Vueva, R.M. Almeida, M. Miola, C. Vitale–Brovarone, E. Verné, W. Höland, J.R. Jones, A unified in vitro evaluation for apatite–forming ability of bioactive glasses and their variants, J. Mater. Sci. Mater. Med. 26 (2015) 115–124.

[29] T. Kokubo, H. Takadama, How useful is SBF in predicting in vivo bone bioactivity? Biomaterials 27 (2006) 2907–2915.

[30] E. Cañas, M.J. Orts, A.R. Boccaccini, E. Sánchez, Microstructural and in vitro characterization of 45S5 bioactive glass coatings deposited by solution precursor plasma spraying (SPPS), Surf. Coat. Technol. 371 (2019) 151–160.

[31] V. López, M. Vicent, E. Bannier, E. Cañas, A.R. Boccaccini, L. Cordero, E. Sánchez, 45S5 bioactive glass coatings by atmospheric plasma spraying obtained from feedstocks prepared by different routes, J. Mater. Sci. 49 (2014) 7933–7942.

[32] T. Poirier, M.P. Planche, O. Landemarre, C. Coddet, Particles spreading phenomena in the case of glass thermal spraying, J. Therm. Spray Technol. 17 (2008) 564–573.

[33] L. Pawlowski, The science and engineering of thermal spray coatings, 2nd ed., John Wiley & Sons, Great Britain, 2008.

[34] D. Yang, Y. Zhang, X. Song, Y. Chen, Z. Shen, C. Yang. Effects of sintering temperature and holding time on porosity and shrinkage of glass tubes, Ceram. Int. 42 (2016) 5906–5910.

[35] J.L. Amorós, M.J. Orts, J. García–Ten, A. Gozalbo, E. Sánchez, Effect of the green porous texture on porcelain tile properties, J. Eur. Ceram. Soc. 27 (2007) 2295–2301.

[36] R.M.C.V. Reis, A.J. Barbosa, L. Ghussn, E.B. Ferreira, M.O. Prado, E.D. Zanotto, Sintering and rounding kinetics of irregular glass particles, J. Am. Ceram. Soc. 102 (2019) 845–854.

[37] R.G. Fernandes, R.M.C.V. Reis, R.R. Tobar, E.D. Zanotto, Simulation and experimental study of the particle size distribution and pore effect on the crystallization of glass powders, Acta Mater. 175 (2019) 130–139.

[38] A. Escardino, M.J. Orts, A. Gozalbo, S. Mestre, J. Aparisi, F. Ferrando, A.J. Ramos, L.F. Sánchez, Porosidad de vidriados pulidos obtenidos por aplicación vía seca (Porosity of polished glazes obtained by dry application), Ceram. Inf. 321 (2005) 74–84.

[39] J. Goldstein, D.E. Newbury, D.C. Joy, C.E. Lyman, P. Echlin, E. Lifshin, L. Sawyer, J.R. Michael, Scanning electron microscopy and X–ray microanalysis, 3rd ed., Springer Science and Bussines Media, The USA, 2003.

[40] A. Cattini, D. Bellucci, A. Sola, L. Pawłowski, V. Cannillo. Suspension plasma spraying of optimised functionally graded coatings of bioactive glass/hydroxyapatite, Surf. Coat. Technol. 236 (2013) 118–126.

[41] J.A. Hernández, J.L. Oteo. Reacciones de la superficie del vidrio con soluciones acuosas, Bol. Soc. Esp. Ceram. Vidr. 21 (1982) 81–97.

[42] E. Cañas, A. Grünewald, R. Detsch, M.J. Orts, E. Sánchez, A.R. Boccaccini, In vitro study of bioactive glass coatings obtained by atmospheric plasma spraying, Bol. Soc. Esp. Céram. Vidr. (2020) DOI: https://doi.org/10.1016/j.bsecv.2020.06.004

[43] M. Cerruti, D. Greenspan, K. Powers, Effect of pH and ionic strength on the reactivity of Bioglass® 45S5, Biomaterials 26 (2005) 1665–1674.

Table 1. Composition of the lab–made bioactive glass (LBG) and the commercial bioactive glass (CBG) powders

Oxide	**SiO_2**	**P_2O_5**	**CaO**	**Na_2O**
LBG powder (wt%)	47.6	5.3	23.1	24.0
CBG powder (wt%)	45.0	6.0	24.5	24.5

Table 2. Plasma spraying parameters used to deposit the TiO_2 bond coat and the bioactive glass top layers

	TiO_2 (bond coat)	**LBG (lab–made bioactive glass)**		**CBG (commercial bioactive glass)**	
Plasma gun	F4–MB	Triplex		Triplex	
Coating refence	——	LBG–SC	LBG–T1	LBG–T2	CBG–T1	CBG–T2
Ar (slpm)	43	25	55	60	55	60
H_2 (slpm)	14	15	——	——	——	——
He (slpm)	——	——	5	——	5	——
Arc current (A)	630	600	400	500	400	500
Gun power (kW)	45	39	38	50	38	50
Plasma enthalpy (kJ/mol)	550	540	520	650	520	650

Table 3. Average thickness and porosity of the resulting coatings

Coating reference	Average thickness (μm)	Percentage of porosity (%)
LBG–SC	100 ± 5	27 ± 3
LBG–T1	95 ± 11	12 ± 2
LBG–T2	101 ± 9	12 ± 2
CBG–T1	94 ± 10	12 ± 1
CBG–T2	99 ± 8	11 ± 1

Table 4. EDX analysis of the coatings before SBF immersion

	LBG (lab–made bioactive glass)			**CBG (commercial bioactive glass)**	
Plasma gun	F4–MB	Triplex		Triplex	
Coating reference	LBG–SC	LBG–T1	LBG–T2	CBG–T1	CBG–T2
SiO_2 (wt%)	50.63	50.29	51.20	50.05	51.96
CaO (wt%)	25.12	27.99	28.55	29.66	31.23
Na_2O (wt%)	20.45	18.63	17.45	17.32	14.28
P_2O_5 (wt%)	3.80	3.09	2.79	2.97	2.53

Figure Captions

Figure 1. FEG–ESEM micrographs of the powder feedstocks. a) lab–made bioactive glass (LBG) and b) commercial bioactive glass (CBG) particles

Figure 2. Cross–section of the obtained coatings at different magnifications. a) and b) LBG–SC coating, c) and d) LBG–T1 coating, e) and f) LBG–T2 coating, g) and h) CBG–T1 coating and i) and j) CBG–T2 coating

Figure 3. The surface of the obtained coatings. a) LBG–SC coating, b) LBG–T1 coating, c) LBG–T2 coating, d) CBG–T1 coating and e) CBG–T2 coating

Figure 4. XRD pattern of all as–sprayed coatings

Figure 5. The surface of the obtained coatings before and after 1, 7 and 14 days of soaking in SBF. a) to d) LBG–SC coating, e) to h) LBG–T1 coating, i) to l) LBG–T2 coating, m) to p) CBG–T1 coating and q) to t) CBG–T2 coating

Figure 6. EDX analysis of the surface of the coatings as–sprayed and after an SBF soaking time of 14 days. a) LBG–SC coating and b) LBG–T2 coating

Figure 7. XRD pattern of the surface of all coatings after 14 days immersed in SBF. Pattern of the LBG–SC coating from [42]

Figure 8. Evolution of P and Ca content of the coatings' surface with soaking time in SBF. Full dots for LBG–SC coating, full triangles for LBG–T1, full squares for LBG–T2, hollow triangles for CBG–T1 and hollow squares for CBG–T2

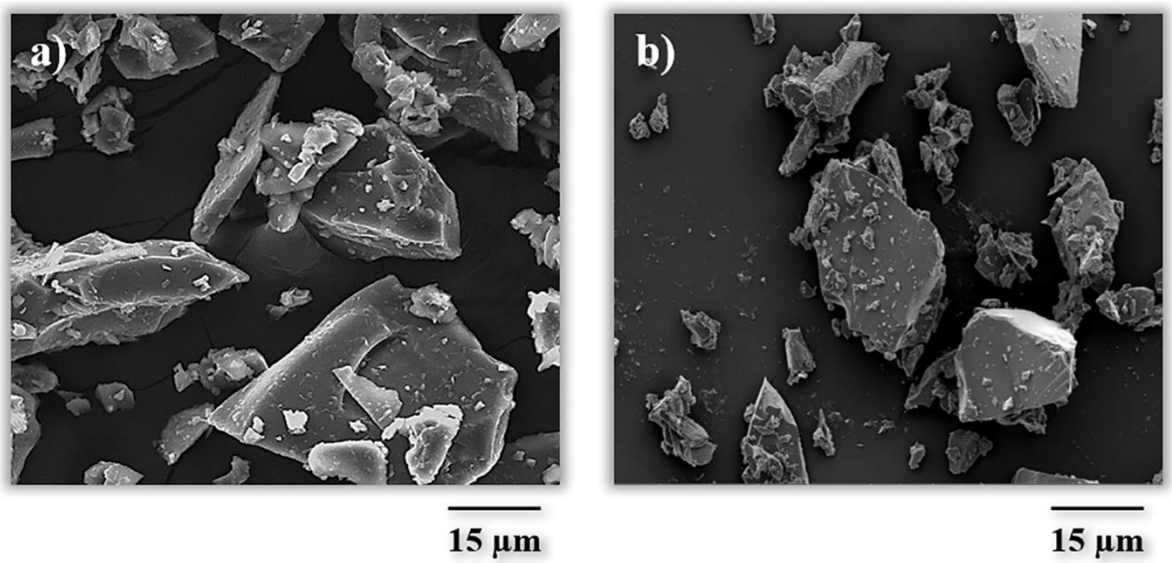

Figure 1

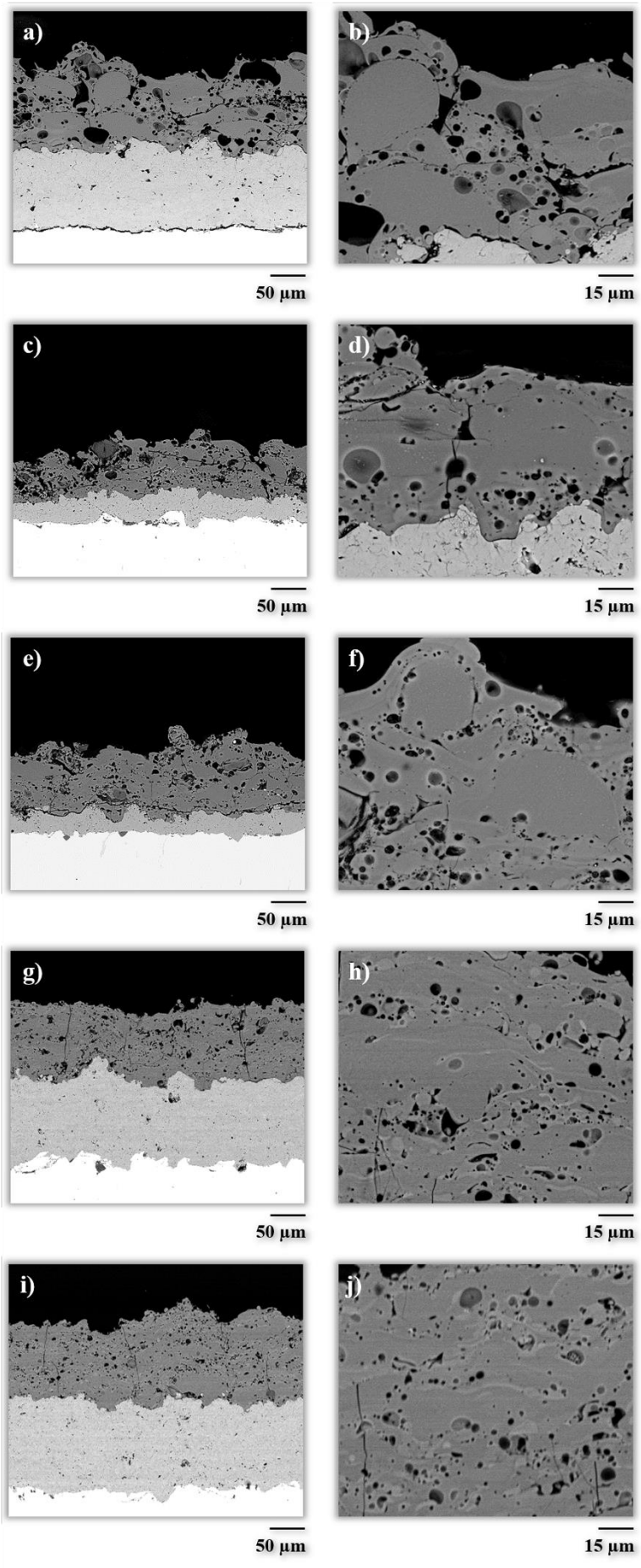
a)
b)
50 µm
15 µm
c)
d)
50 µm
15 µm
e)
f)
50 µm
15 µm
g)
h)
50 µm
15 µm
i)
j)
50 µm
15 µm

Figure 2

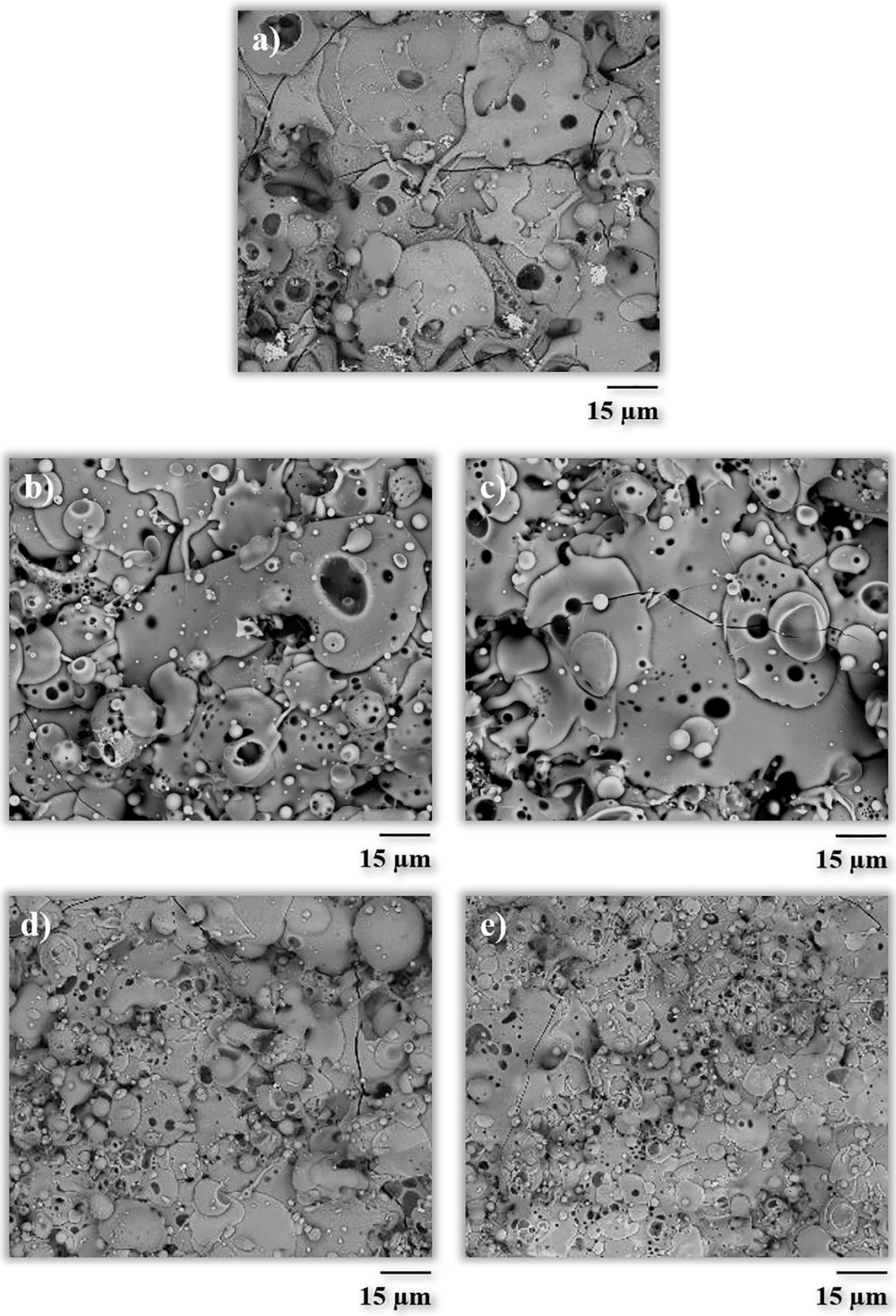

Figure 3

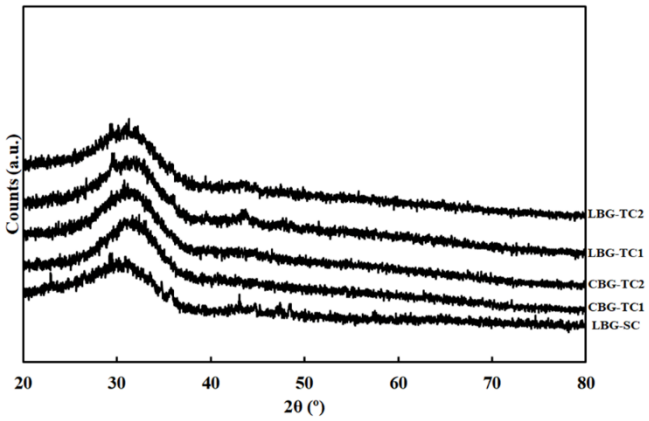
Counts (a.u.)
LBG-TC2
LBG-TC1
CBG-TC2
CBG-TC1
LBG-SC
20
30
40
50
60
70
80
2θ (°)

Figure 4

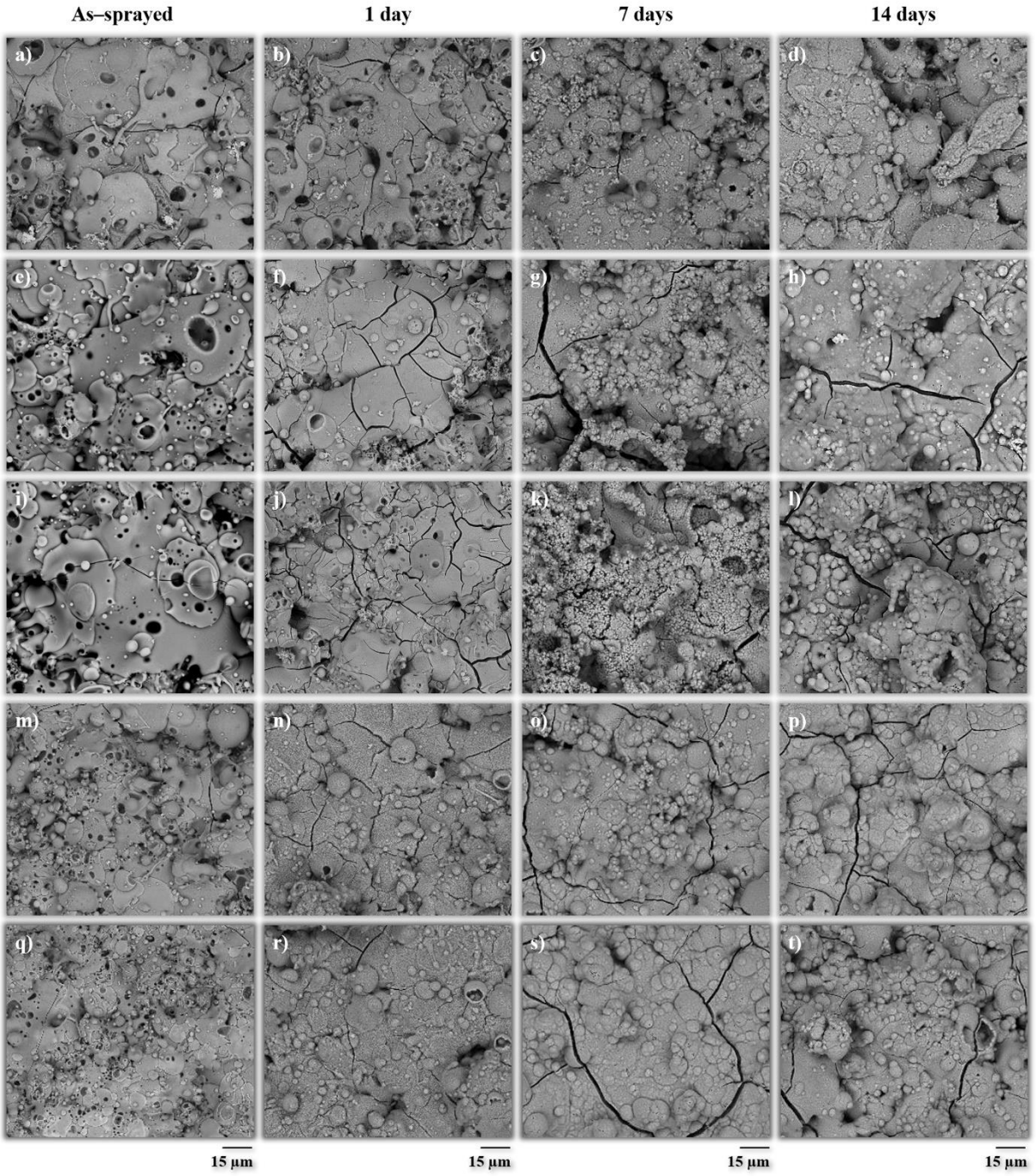
As–sprayed
1 day
7 days
14 days
a)
b)
c)
d)
e)
f)
g)
h)
i)
j)
k)
l)
m)
n)
o)
p)
q)
r)
s)
t)
15 µm
15 µm
15 µm
15 µm

Figure 5

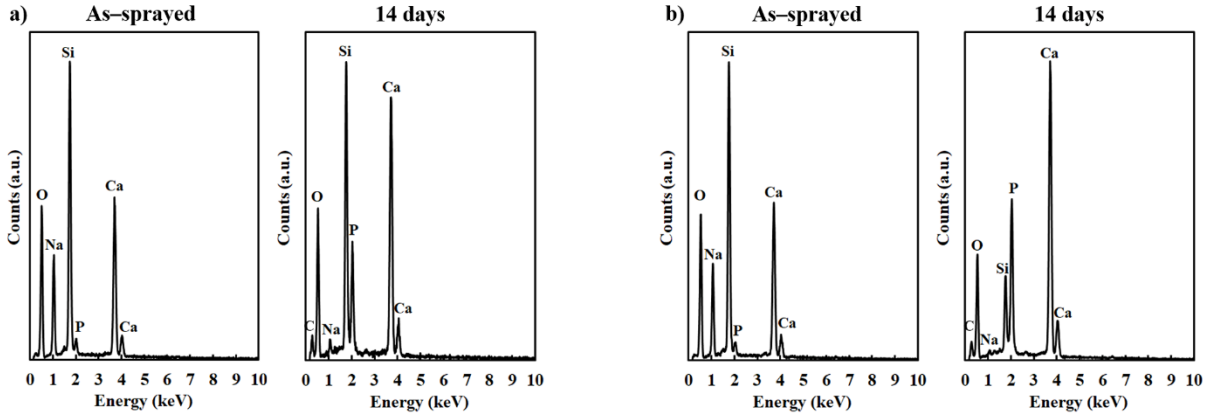
a)
As–sprayed
14 days
b)
As–sprayed
14 days
Counts (a.u.)
Energy (keV)
O
Na
Si
P
Ca
C
0 1 2 3 4 5 6 7 8 9 10

Figure 6

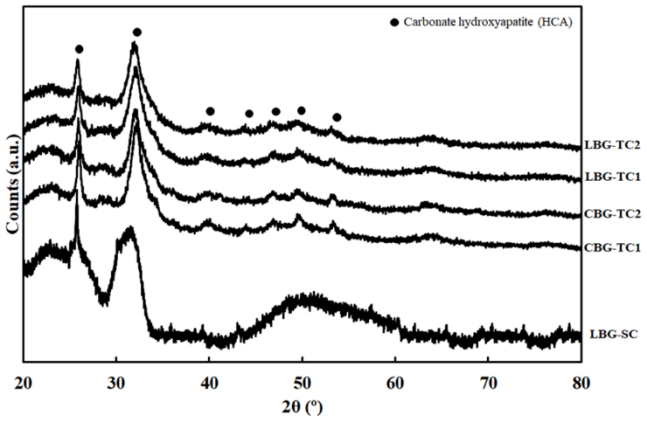
● Carbonate hydroxyapatite (HCA)
LBG-TC2
LBG-TC1
CBG-TC2
CBG-TC1
LBG-SC
Counts (a.u.)
20
30
40
50
60
70
80
2θ (°)

Figure 7

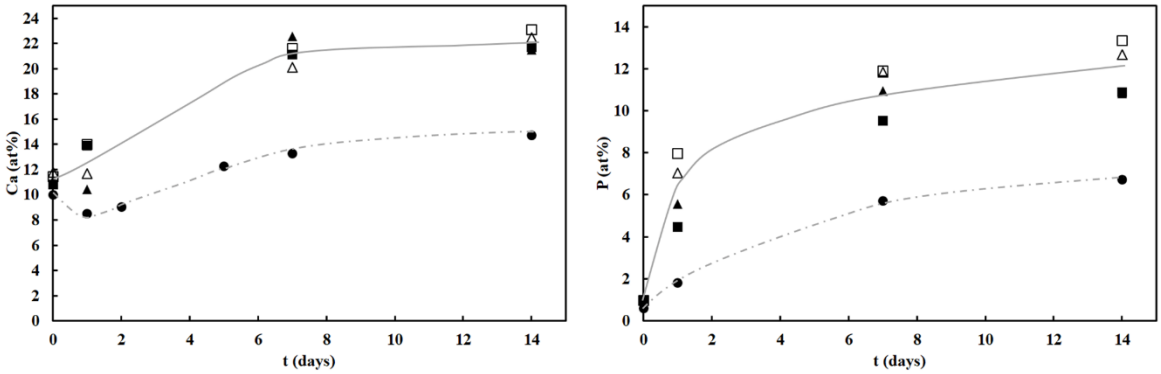

Figure 8